

## Supporting Information

### **Simplifying and accelerating kinetics enabling fast-charge Al battery**

Minglei Mao,<sup>#†</sup> Ze Yu,<sup>#†</sup> Zejing Lin,<sup>†</sup> Yong-Sheng Hu,<sup>†</sup> Hong Li,<sup>†</sup> Xuejie Huang,<sup>†</sup>  
Liquan Chen<sup>†</sup> Miao Liu,<sup>\*†‡§</sup> Liumin Suo,<sup>\*†‡Δ</sup>

<sup>†</sup>Beijing Advanced Innovation Center for Materials Genome Engineering, Key Laboratory for Renewable Energy, Beijing Key Laboratory for New Energy Materials and Devices, Institute of Physics, Chinese Academy of Sciences, Beijing 100190, China

<sup>‡</sup>Center of Materials Science and Optoelectronics Engineering, University of Chinese Academy of Sciences, Beijing 100049, China

<sup>Δ</sup>Yangtze River Delta Physics Research Center Co. Ltd., Liyang, Jiangsu 213300, China

<sup>§</sup>Songshan Lake Materials Laboratory, Dongguan, Guangdong 523808, China

\*Email: [mliu@iphy.ac.cn](mailto:mliu@iphy.ac.cn), [suoliumin@iphy.ac.cn](mailto:suoliumin@iphy.ac.cn)

**Material Synthesis:**

Tetra-(phthalimido)-benzoquinone was prepared according to previous reports with some modifications.<sup>1</sup> In a typical procedure, 0.2 mol tetrachloro-1, 4-benzoquinone (99%, Sigma-Aldrich) and 0.8 mol potassium phthalimide (99%, Sigma-Aldrich) was dissolved in 500 mL acetonitrile (ACN, HPLC gradient grade, Sigma-Aldrich). The reaction mixture was refluxed with stirring for 12 h under argon atmosphere and collected by centrifugation. Subsequently, the solid was dissolved into 200 mL Dimethylformamide (AR, Acros), stirred at 100 °C for 10 min, and centrifuged to get brown-yellow powder. The powder was washed with deionized water at 90 °C for three times followed by drying at 60 °C overnight under vacuum.

**Material Characterizations:**

The XRD patterns were measured using Cu K $\alpha$  radiation on an X'Pert Pro MPD X-ray diffractometer from 5° to 40° (2 $\theta$ ). The morphologies of samples were investigated by a SEM (Hitachi S-4800) with energy-disperse X-ray analysis. The chemical composition was investigated by the energy-dispersive spectroscopy (EDS). Mass spectra and liquid chromatogram were acquired using liquid Chromatograph Mass Spectrometer (LC-MS) recorded on Xevo G2-XS QToF. Mass spectra were acquired under negative mode with the cone voltage and capillary voltage of 40.0 V and 2.0 kV in negative ion mode respectively. For liquid chromatogram, the column temperature and flow rate were set to 55 °C and 0.4 mL/min respectively, with TPBQ dissolved into ACN (acetonitrile) as the mobile phase. <sup>13</sup>C-NMR spectrum was obtained by Bruker AVANCE III 400MHz. Thermogravimetric analysis (TGA) was measured from 30 to 800 °C at a heating rate of 10 °C/min under 80 mL/min of flowing Ar with a Perkin-Elmer TGA 4000. The X-ray photoelectron spectroscopy (XPS) spectra were recorded with a spectrometer having Mg/Al K $\alpha$  radiation (ESCALAB 250 Xi, Thermo Fisher). All binding energies reported were corrected using the signal of the carbon at 284.8 eV as an internal standard. Raman measurements were performed on a Horiba Jobin Yvon Labram Aramis using a 532 nm diode-pumped solid-state laser, attenuated to give  $\approx$ 900  $\mu$ W power at the sample surface. Fourier transform infrared spectra (FT-IR) were recorded on a NEXUS 670 FTIR Instrument. For ex situ XPS and FT-IR measurements, pouch cells with different condition were disassembled in an argon-filled glove box and the electrodes were washed in tetrahydrofuran (anhydrous, Alfa Aesar, 99.9%) for three times to remove the electrolyte, then the drying samples were obtained and moved to the machine

with Argon-filled sealing tube as transferred box. In this process, all samples were exposed to air within 3-4 s.

### **Electrochemical Measurements:**

Cell assembly was carried out in an Ar-filled glovebox with O<sub>2</sub> and H<sub>2</sub>O levels below 0.1 ppm. TPBQ electrodes were prepared by compressing the as-prepared powders, graphene, ketjen black, PTFE at a weight ratio of 5:1:3:1 onto the molybdenum grid. The loading mass of electrodes is ~2 mg/cm<sup>2</sup>. Rechargeable Al batteries (RABs) were assembled using pouch cells with AlCl<sub>3</sub>-1-ethyl-3-methyl-imidazolium chloride (EMImCl) ionic liquid electrolyte (molar ratio of AlCl<sub>3</sub>: EMImCl is 1.3), polished Al metal as the anode, and Whatman glass fibers as separators. The electrochemical test was conducted on LAND-CT2001A battery test station (LAND Electronic Co.) with voltage cutoff of 0.5-2.3V at room temperature. During GITT measurement, the electrode was discharged/charged at a pulse current of 20 mA/g for the duration of 1h followed by a relaxation of 2h at open circuit to reach equilibrium potentials. Cyclic voltammograms (CVs) were carried out using a Parstat 263A electrochemical workstation (AMETEK Co.). Nyquist plots were recorded using Autolab PGSTAT302N (Metrohm, Switzerland) at a frequency range of 0.01-100 kHz.

### **Electrical Conductivity Measurements**

The electrical conductivity of TPBQ electrodes is performed using a four-pin probe (Kyowa Electronic Instruments Co., Ltd., Japan) according to MCP-PD51. By passing a current through two outer probes and measuring the voltage through the inner probes allows the measurement of the substrate resistivity.<sup>2</sup> The probe's pin has a 0.7-mm diameter, a 3-mm inter-pin spacing, and 10-mm sample radius. A total of four samples with mass of ~2 grams are used. The four pins penetrate the sample via a constant pressure as seen in Table S1-S4, and the resistivity ( $\rho$ ) that is yielded from the test is then used to compute the electrical conductivity ( $\sigma$ ) with the equation as follows

$$\sigma = \frac{1}{\rho}$$
$$\rho = \frac{V}{I} \frac{\pi t}{\ln\left(\frac{\sinh(t/s)}{\sinh(t/2s)}\right)}$$

Where  $V$  is the voltage across inner probes,  $I$  is the current in outer probes,  $t$  is the layer thickness in cm,  $s$  is the probe spacing.

### Computational Details

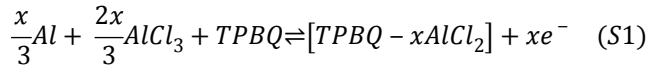
The first-principles calculations were employed to investigate the structure information, adsorption sites and reaction pathway of TPBQ in RABs. In detail, density functional theory (DFT) calculations are performed using the Vienna ab-initio simulation Package (VASP), in which the Perdew-Burke-Ernzerhof (PBE) flavor of pseudopotential (within the generalized gradient approximation (GGA) framework) is selected to describe the exchange and correlation functional of the system. The pseudopotentials are generated using projector-augmented wave (PAW) method and provided along with the Vienna ab-initio simulation Package (VASP). All structures are fully relaxed to reach the energy convergence criteria ( $\leq 1\text{E-}5$  eV) and force convergence criteria ( $\leq 0.02$  eV/Å for each atom). A rod model is adopted in order to describe the TPBQ stacking. Vacuum spacing is larger than 15 Å to prevent the atoms from interacting with their periodical images. The energy cutoff of 450 eV and k-grid mesh of  $1 \times 1 \times 2$  are used throughout this work. DFT-D2 of Van der Waals (vdW) treatment is applied as the system is vdW active.

From measured XRD patterns, TPBQ are well crystalized. In order to figure out the crystalline structure of TPBQ, two steps are taken: (1) identify the spatial configuration of a single TPBQ molecule and (2) pack the molecules in a thermodynamic-favorable manner to obtain the TPBQ crystal. The first step follows a computational workflow that run the energy minimization algorithm to yield the initial optimized structure. Ab-initio molecular dynamics (MD) simulation is used to ensure the stability of modeling structure at room temperature. Accordingly, two structures named by “S-1” and “S-2” might actually exist (Figure S4). Thus, “S-1” and “S-2” are used as building blocks to assemble layered TPBQ crystal by stacking TPBQ molecules along  $c$  direction.

To cover all possible configurations, basic building blocks are allowed to rotate when stacking TPBQ molecules. It ends with two stacking patterns: non-rotated and 90°-rotated in  $a$ - $b$  plane (Figure S5). Therefore, four supercells are achieved, corresponding to four possible crystal structures named by “S-1n”, “S-1r”, “S-2n” and “S-2r”. The structure “S-1n”, “S-1r” and “S-2n” are thermodynamically stable in contrast to the unstable “S-2r” due to the high formation energy of +0.61 eV. We performed DFT-level energy minimization, Raman/infrared spectroscopy

calculations, XRD patterns calculations, and redox-mechanism investigation for the four structures.

To investigate the redox potential of TPBQ,  $AlCl_2^+$  is placed in various absorption sites. We calculate the total energy of precursors and products during the adsorption process. Based on the electrochemical reaction equation S1, the redox potential of TPBQ can be computed using the equation S2.



$$V = - \frac{3E(TPBQ - xAlCl_2) - 3E(TPBQ) - xE(Al) - 2xE(AlCl_3)}{3xe} \quad (S2)$$

where  $V$  is the redox potential,  $E(TPBQ-xAlCl_2)$  is the energy of TPBQ absorbed with  $AlCl_2$  ( $0 < x \leq 4$ ),  $E(TPBQ)$  is the energy of basic structure,  $E(Al)$  is the energy of aluminum,  $E(AlCl_3)$  is the energy of aluminum chloride,  $e$  is the charge of ions (+3 for Al).

The theoretical capacity can be calculated using Nernst Equation as follows:

$$C = \frac{n * F}{3.6M_w} \quad (S3)$$

where  $n$  is the number of electron transferred,  $F$  is the Faraday's constant ( $F=96486$  C/mol), and  $M_w$  is the relative molecular mass (688 g/mol for TPBQ).

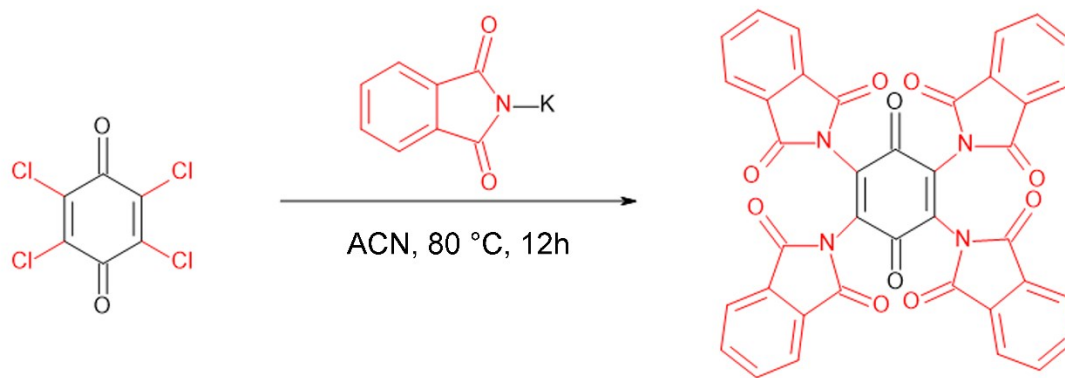


**Figure S1.** The preparation process of 2, 3, 5, 6-tetraphthalimido-*p*-benzoquinone (TPBQ).

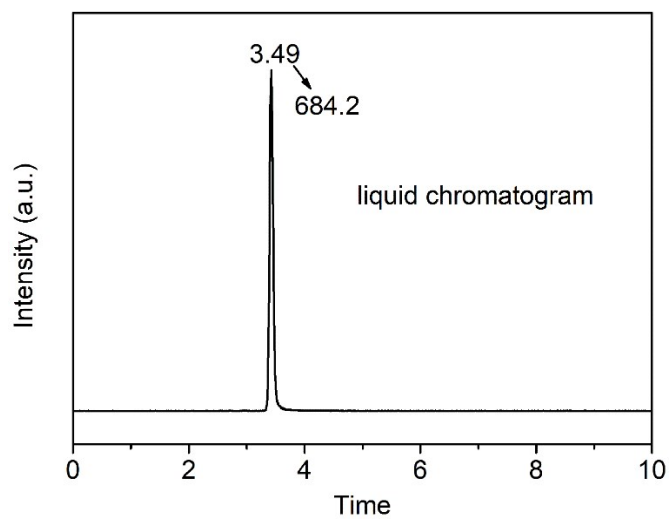


**Figure S2.** Liquid chromatogram of TPBQ. The retention time of 3.49 corresponds to its molecular weight of 684.2.

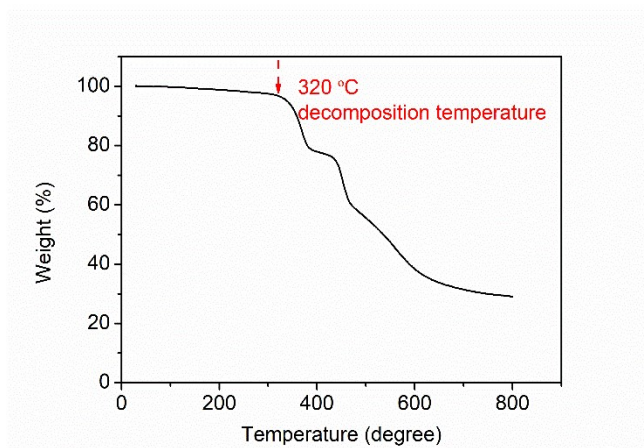


**Figure S3.** TGA curve of pristine TPBQ from 30 to 800 °C at 10 °C/min under Ar. The decomposition temperature of TPBQ is around 320 °C, indicating the good thermal stability.

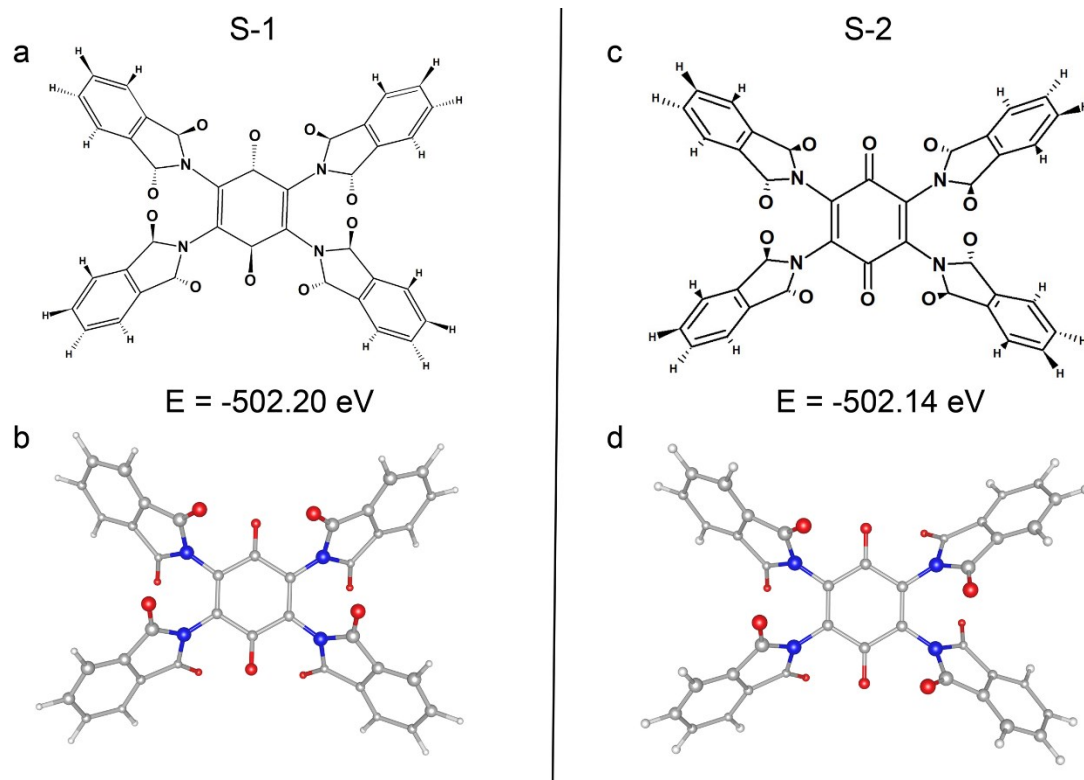


**Figure S4.** Two structures of TPBQ molecular viewed from the direction of c. (a, b) Structure-1 (S-1) and (c, d) Structure-2 (S-2). (a) and (c) are prepared by Chems sketch, while (b) and (d) are prepared by VESTA. Inset is the structure energy.

Close energy of S-1 ( $E = -502.20$  eV) and S-2 ( $E = -502.14$  eV) indicates that two structures might actually exist.

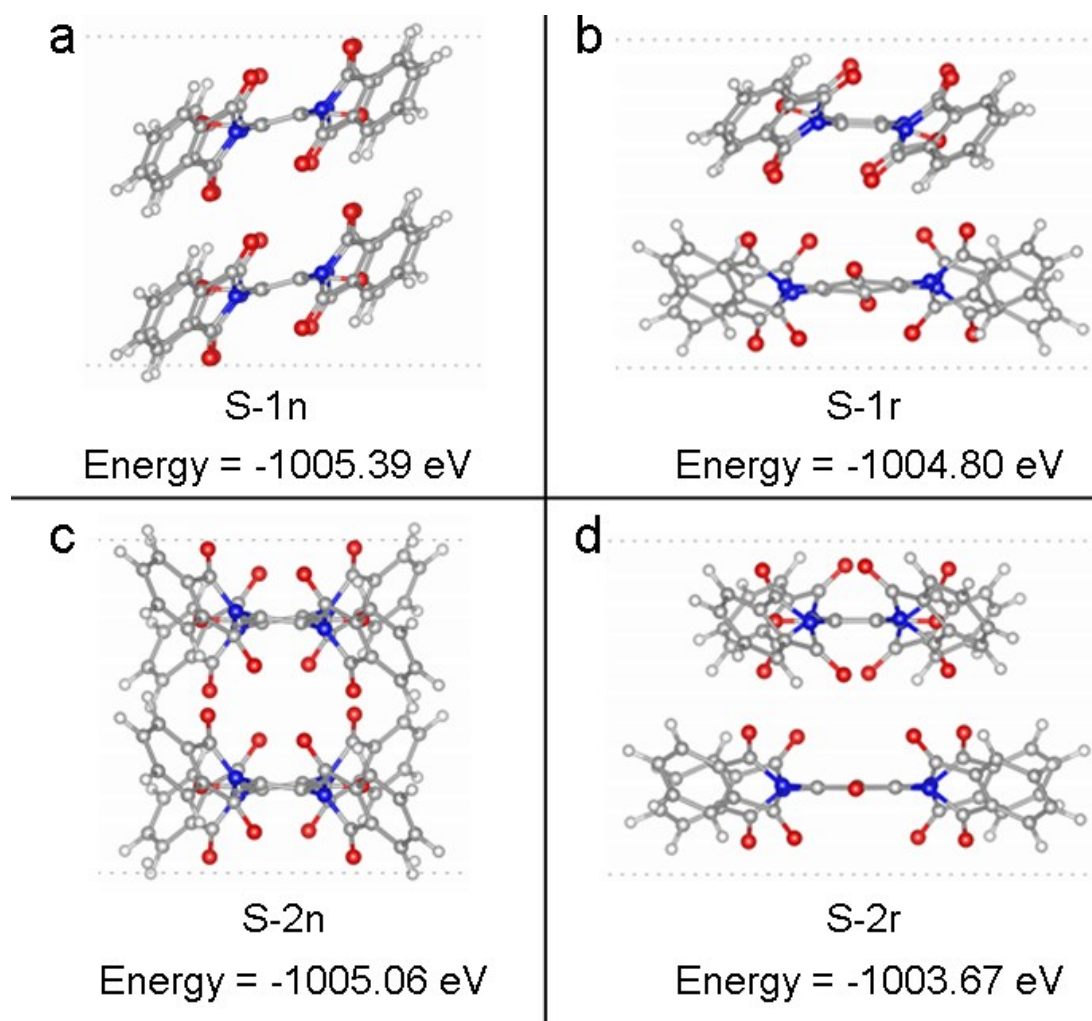


**Figure S5.** Four TPBQ supercells viewed from direction a. (a) non-rotated (S-1n) and (b) 90°-rotated (S-1r) constructed by S-1 molecular, (c) non-rotated (S-2n) and (d) 90°-rotated (S-2r) constructed by S-2 molecular. Images prepared with VESTA. Inset is the structure energy. Accordingly, the formation energy of “S-1n”, “S-1r”, “S-2n”, and “S-2r” are calculated to be -0.99, -0.40, -0.78, and 0.61 eV/molecule, respectively.

Intuitively, the supercell of S-1n will anticlockwise deflect approximately 15° in b-c plane upon optimization, likely due to the spatial position of oxygen atoms in the structure. The structure “S-2r” is thermodynamically unstable due to the high formation energy of + 0.61 eV/molecule.

$$E(\text{formation energy}) = E(\text{supercell/molecule}) - 2 * E(\text{TPBQ/molecule}).$$

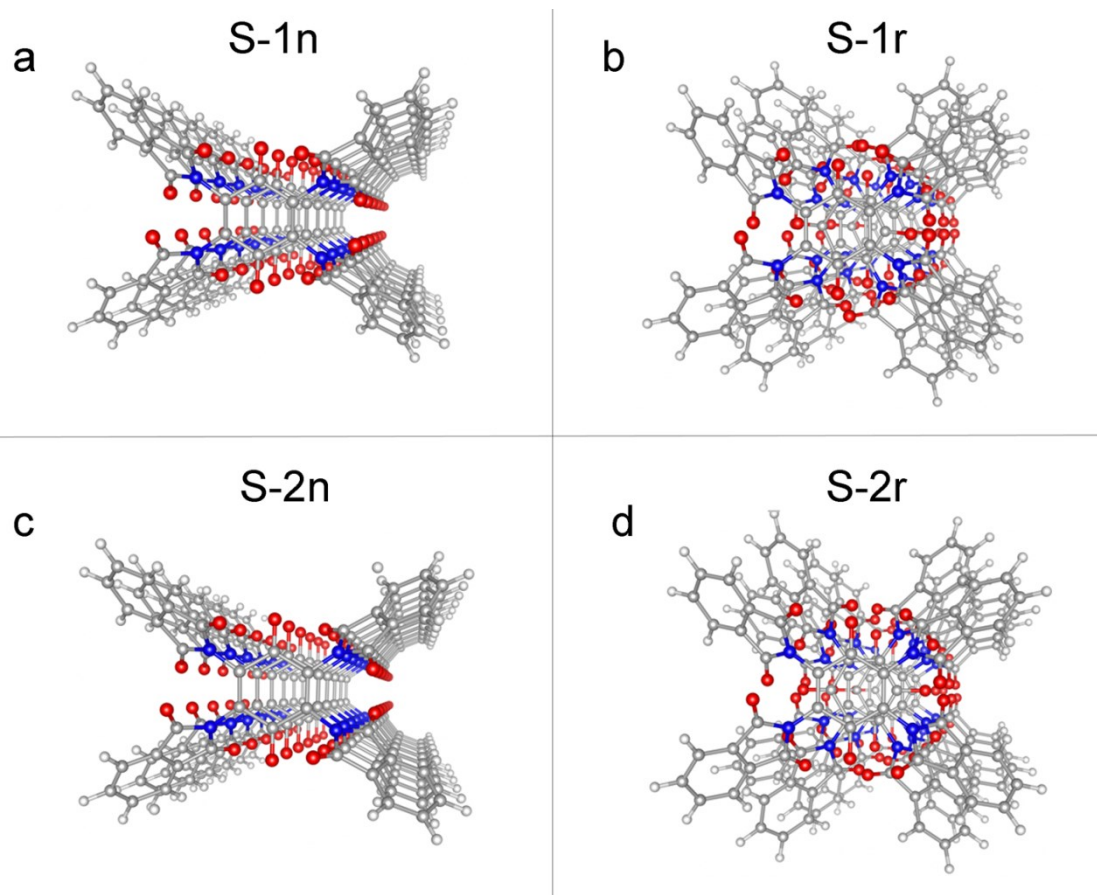


**Figure S6.** Periodic display of TPBQ modeling structures by expanding the supercell in the direction of *c*: (a) S-1n, (b) S-1r, (c) S-2n, (d) S-2r. Images prepared with VESTA.

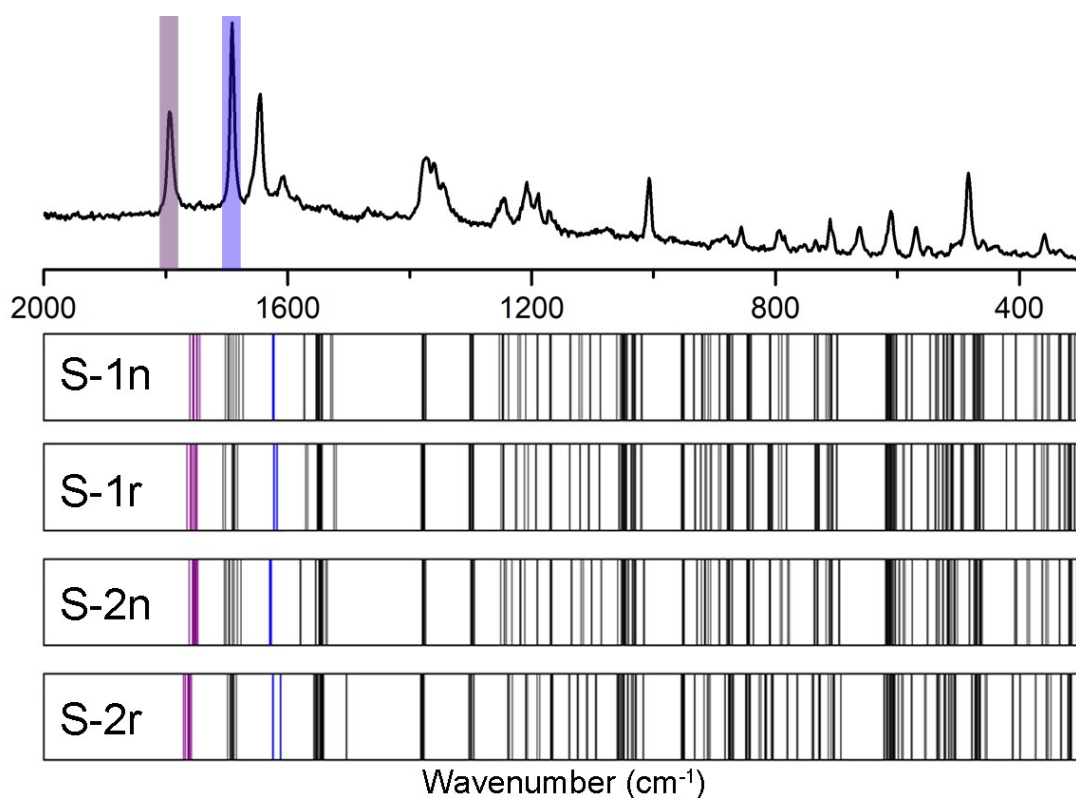


**Figure S7.** Measured Raman spectra of TPBQ and Raman-infrared spectrum of modeling structures from DFT calculations: S-1n, S-1r, S-2n, and S-2r. The purple and blue color represent imide and quinonyl  $-C=O$ , respectively.

The calculated Raman-infrared spectra of modeling structures match well with the measured one of TPBQ, especially for imide (purple color) and quinonyl (blue color)  $-C=O$  with the deviation within ten centimeters.

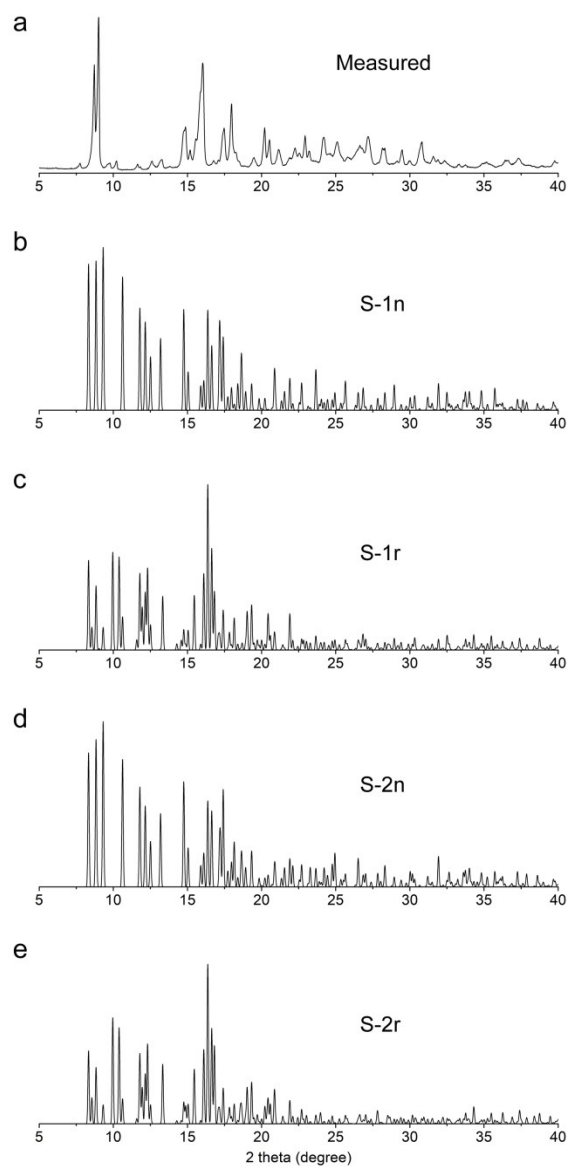


**Figure S8.** XRD patterns of TPBQ: (a) measured one and (b-e) modeling ones from DFT calculations.

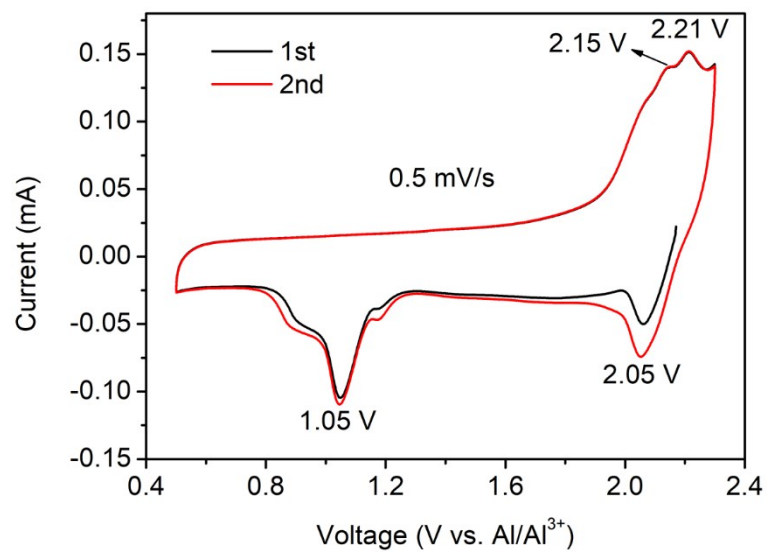


**Figure S9.** Typical cyclic voltammograms of TPBQ for the first 2 cycles between 0.5-2.3 V at 0.5 mV/s.

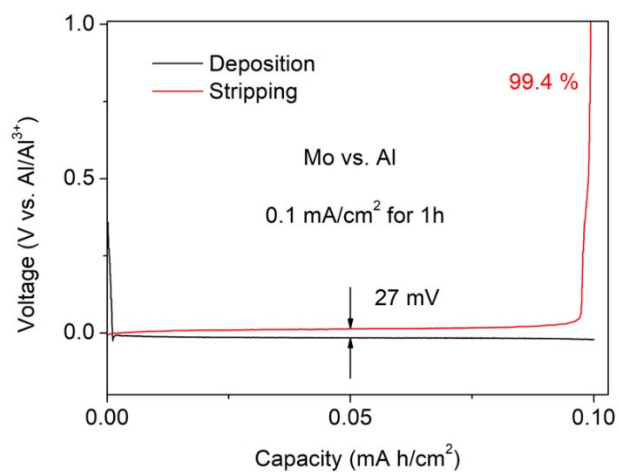


**Figure S10.** Electrochemical performance of Al plating/stripping on a Mo working electrode using AlCl<sub>3</sub>-[EMIm]Cl ionic liquid electrolyte. Current density: 0.1 mA/cm<sup>2</sup>. The coulombic efficiency (CE) of Al plating/stripping is 99.4% with the overpotential of ~13.5 mV (half of 27 mV).

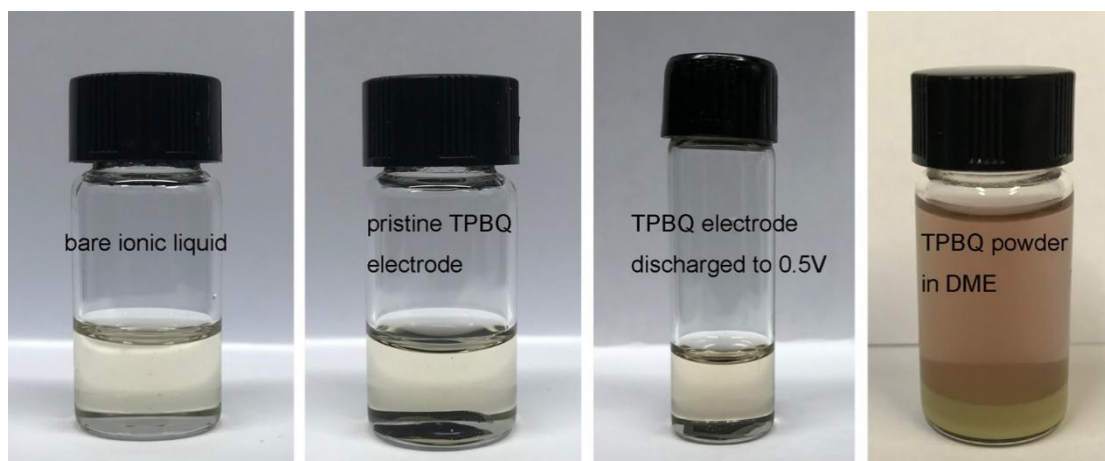


**Figure S11.** Digital images of pristine and fully discharged TPBQ immersed in RABs electrolyte ( $\text{AlCl}_3$ -[EMIm]Cl ionic liquid). Digital images of bare ionic liquid and pristine TPBQ powder immersed in DME are also provided for comparison.

No apparent color change can be observed in both pristine and discharged TPBQ electrodes in  $\text{AlCl}_3$ -[EMIm]Cl ionic liquid, indicating that TPBQ hardly dissolve into RABs electrolyte, accounting for its superior cyclability in RABs. In comparison, TPBQ will readily dissolve into non-aqueous solvent (DME), indicated by apparent color change of DME.

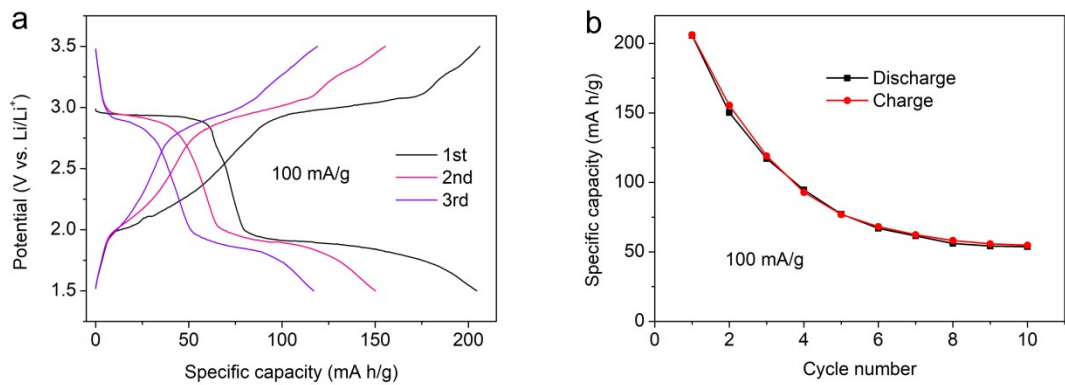


**Figure S12.** Electrochemical performance of TPBQ in LIBs with LiTFSI/DME as the electrolyte and metallic Li as the anode at 100 mA/g between 1.5 and 3.5 V. (a) The first three discharge/charge curves and (b) cycling performance for the first ten cycles.

The initial discharge and charge capacity of TPBQ in LIBs are 204 and 201 mA h/g, respectively, with two discharge plateaus of  $\sim 3\text{V}$  and  $2\text{V}$  (Figure S12a). The plateaus sharply shorten in the first three cycles, accompanied by the capacity decay to 120 mA h/g in the third cycles. A poor cycling stability of TPBQ can be observed within 10 cycles (Figure S12b), which is probably ascribed to high dissolution of TPBQ into LIBs electrolyte (LiTFSI/DME) (Figure S11).

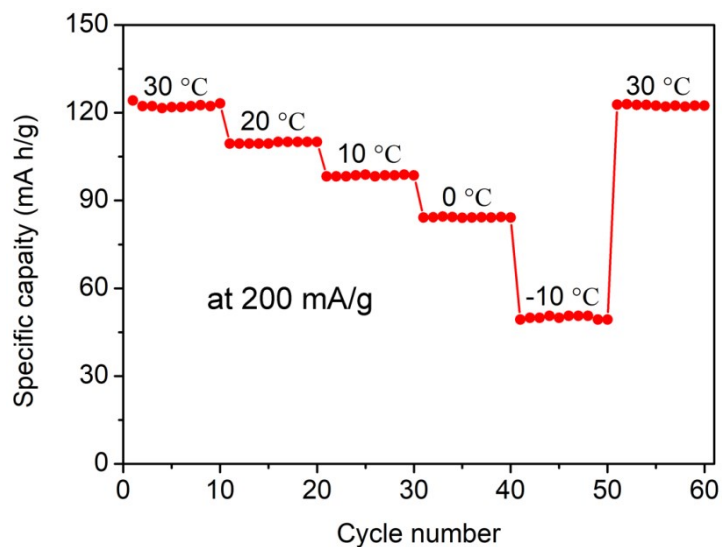


**Figure S13.** Temperature dependence of specific capacities of TPBQ/Al pouch cells from 30 to -10 °C at 200 mA/g.

The fast reaction kinetics and excellent rate performance of TPBQ/Al pouch cells motivate us to investigate its low-temperature performance. From 30 to 0 °C, the capacity of TPBQ/Al pouch cells gradually decreases from 120 to 84 mA h/g at 200 mA/g. Even at -10 °C, a capacity of 50 mA h/g remains, demonstrating the good low-T performance. Lower temperature (< -20 °C) will solidify the ionic liquid electrolyte, which cannot support TPBQ/Al pouch cells to work.

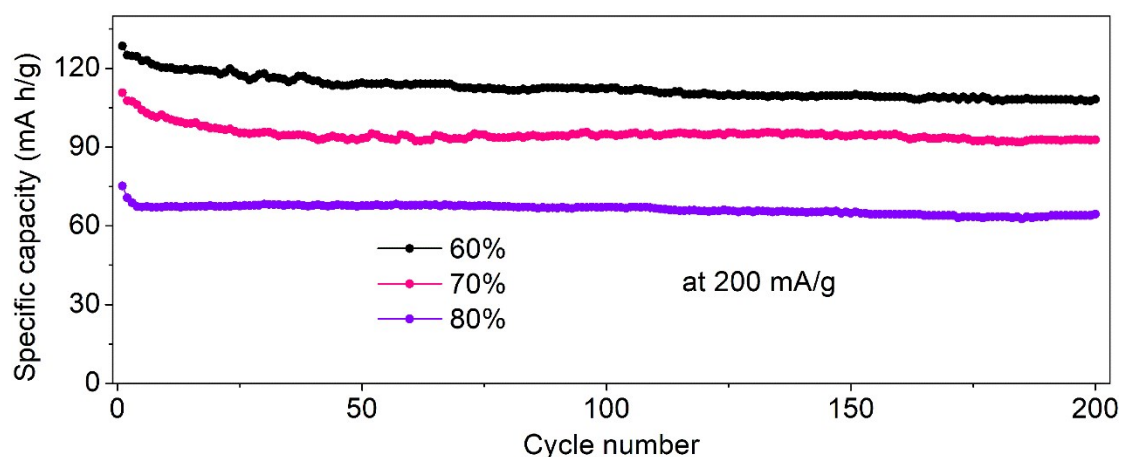


**Figure S14.** Cycling performance with various TPBQ ratio of 60%, 70%, and 80% at 200 mA/g. Loading mass: 2 mg/cm<sup>2</sup>.

The electrochemical performance of electrodes with higher TPBQ ratios (from 60% to 80%) is evaluated, in which all the electrodes exhibit good cycling stability within 200 cycles at 200 mA/g. When TOBQ ratios increase from 60% to 80%, the capacities decrease from 106.2 mA h/g to 64.4 mA h/g, which could be ascribed to lower electrical conductivity of electrodes with high TPBQ ratio, confirmed by four-probe method (Figure S15a and Table S1-S4) and electrochemical impedance spectroscopy (EIS) results (Figure S15b).

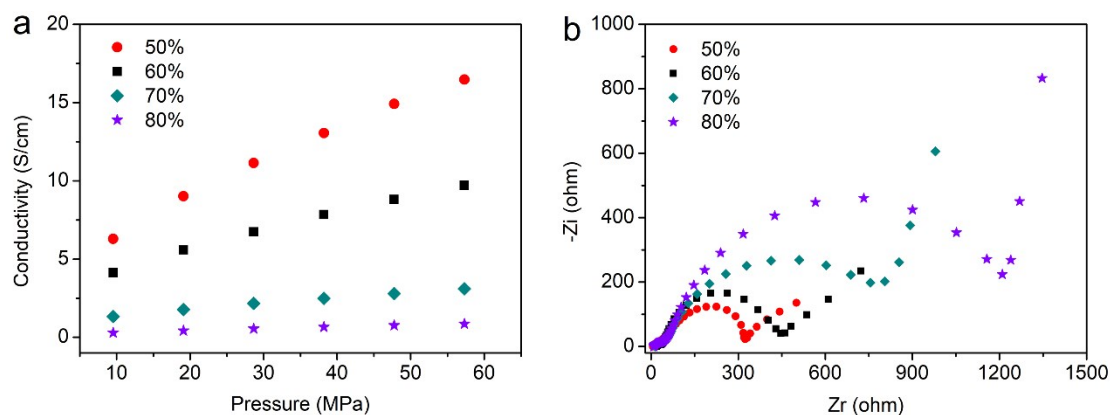


**Figure S15.** (a) The electrical conductivity of TPBQ electrodes with various TPBQ ratios (50%-80%) under various pressure (from 10 to 60 MPa) using four-probe method. Details are referred to Table S1-S4. (b) EIS of TPBQ electrodes with various TPBQ ratios at a frequency range of 0.01-100 kHz.

To investigate reasons for higher TPBQ ratio leading to lower capacities, the electrical conductivity of electrodes with various TPBQ ratios was studied by four-probe method and electrochemical impedance spectroscopy (EIS). In four-probe method, the electrical conductivity of TPBQ electrodes decreases with the content of TPBQ increasing (the content of carbon decreasing) under all pressure tested (Figure S15a), which is further confirmed by EIS. EIS of pristine TPBQ/Al pouch cells display that the charge-transfer resistance (corresponding to the second semicircles in Figure S15b) increases with more TPBQ, indicating the decline of electrical conductivity.

**Table S1.** The results of the electrical conductivity measurements of 50% TPB.

No.	Load (kN)	Pressure (MPa)	Thickness (mm)	Volume resistivity (Ohm/cm)	Conductivity (S/cm)	Density (g/cc)
1	3.00	9.55	7.50	0.1588	6.296	0.5233
2	6.00	19.10	6.25	0.1108	9.022	0.6280
3	9.00	28.65	5.58	0.08974	11.14	0.7034
4	12.00	38.20	5.10	0.0766	13.05	0.7696
5	15.00	47.75	4.72	0.06702	14.92	0.8315
6	18.00	57.30	4.45	0.06071	16.47	0.8820

**Table S2.** The results of the electrical conductivity measurements of 60% TPB.

No.	Load (kN)	Pressure (MPa)	Thickness (mm)	Volume resistivity (Ohm/cm)	Conductivity (S/cm)	Density (g/cc)
1	3.00	9.55	6.86	0.2424	4.126	0.7424
2	6.00	19.10	5.98	0.1794	5.575	0.8217
3	9.00	28.65	5.45	0.1483	6.741	0.9345
4	12.00	38.20	5.05	0.1275	7.841	1.009
5	15.00	47.75	4.75	0.1134	8.818	1.072
6	18.00	57.30	4.51	0.1030	9.709	1.129

**Table S3.** The results of the electrical conductivity measurements of 70% TPB.

No.	Load (kN)	Pressure (MPa)	Thickness (mm)	Volume resistivity (Ohm/cm)	Conductivity (S/cm)	Density (g/cc)
1	3.00	9.55	8.10	0.751	1.332	0.7899
2	6.00	19.10	7.30	0.5634	1.775	0.8764
3	9.00	28.65	6.77	0.4608	2.17	0.9451
4	12.00	38.20	6.40	0.4011	2.493	0.9997
5	15.00	47.75	6.11	0.3575	2.797	1.047
6	18.00	57.30	5.85	0.3227	3.099	1.094

**Table S4.** The results of the electrical conductivity measurements of 80% TPB.

No.	Load (kN)	Pressure (MPa)	Thickness (mm)	Volume resistivity (Ohm/cm)	Conductivity (S/cm)	Density (g/cc)
1	3.00	9.55	6.48	3.483	0.2871	0.8842
2	6.00	19.10	5.86	2.370	0.4220	0.9777
3	9.00	28.65	5.46	1.836	0.5446	1.049
4	12.00	38.20	5.17	1.517	0.6590	1.108
5	15.00	47.75	4.95	1.324	0.7554	1.157
6	18.00	57.30	4.77	1.176	0.8502	1.201

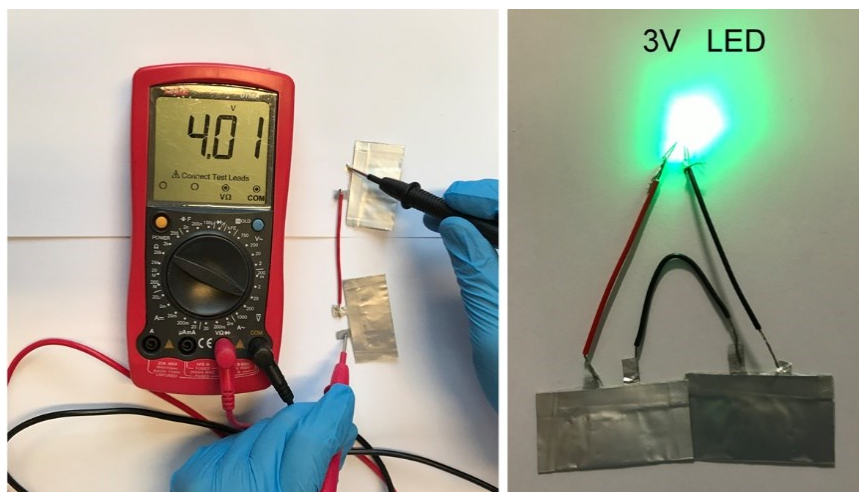


**Figure S16.** The application of two TPBQ/Al pouch cells in series with 4V voltage output powering a 3V-LED light.

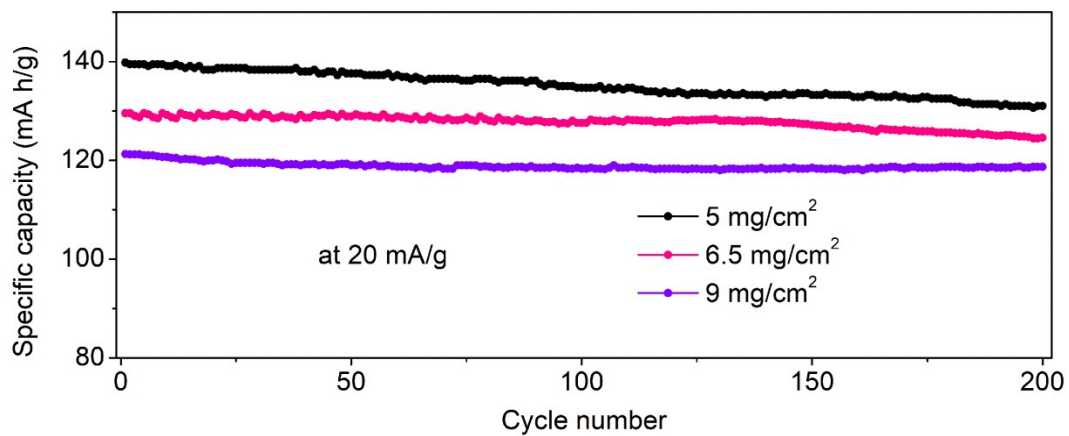


**Figure S17.** Cycling performance of TPBQ/Al pouch cells based on mass specific capacity with various loading mass (5 mg/cm<sup>2</sup>, 6.5 mg/cm<sup>2</sup>, and 9 mg/cm<sup>2</sup>) at 20 mA/g for the first 200 cycles.



**Figure S18.** The optical photograph of TPBQ-Al pouch cells.

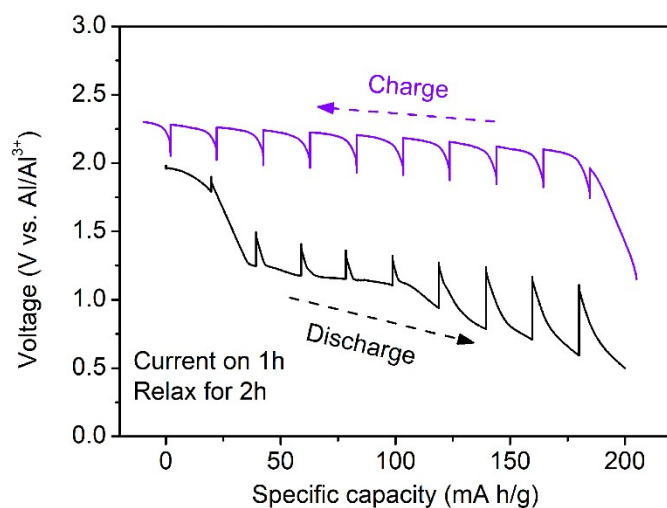


**Figure S19.** Quasi-equilibrium voltage profile of TPBQ/Al pouch cells obtained from GITT. The cells were allowed to relax for 2h after each 1h discharging or charging at 20 mA/g and RT.

Galvanostatic intermittent titration technique (GITT) was conducted to investigate the reaction kinetics of TPBQ/Al pouch cells. GITT can provide both thermodynamic hysteresis and kinetic polarization.<sup>3</sup> The cells were discharged or charged at 20 mA/g for 1h followed by 2h relaxation at an open circuit to reach quasi-equilibrium. The cumulative discharge capacity is 200 mA h/g, slightly more than that in galvanostatic discharge/charge process. The overpotentials of TPBQ for the 1<sup>st</sup> and 2<sup>nd</sup> discharge plateaus are ~105 mV and 207 mV, respectively, while that for charge plateau is ~259 mV, indicating the slower reaction kinetics of charge process.

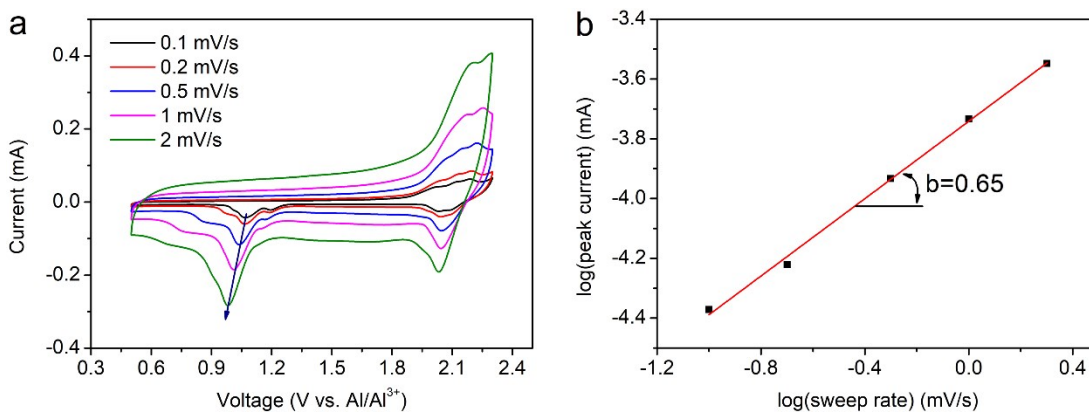


**Figure S20.** (a) Cyclic voltammograms of TPBQ/Al pouch cells at various scan rates ranging from 0.1 to 2 mV/s between 0.5 and 2.3V. (b) The log(*i*) versus log(*v*) plot of the cathodic current response at ~1.1 V (versus Al/Al<sup>3+</sup>). The slope of this line gives the *b* value to be 0.65.

The control step of the reaction kinetics was investigated using cyclic voltammetry (CV) at various scan rates. The stepwise increase of scan rates from 0.1 to 2 mV/s shows only a small increase in polarization (Figure S20a), indicating the inherently fast reaction kinetics of TPBQ. In theory, the peak current (*i*) at a fixed potential obeys a power-law relationship with the sweep rate (*v*).<sup>4,5</sup>

$$i = av^b \quad (\text{I})$$

For a redox reaction limited by semi-infinite diffusion, the peak current *i* follows a linear relationship with  $v^{0.5}$  ( $b = 0.5$ ), while for a complete surface-controlled process, it varies with  $v$  ( $b = 1$ ).<sup>6</sup> The linear fit of common logarithm relationship of peak current and scan rate displays that *b* value for TPBQ is 0.65 (Figure S20b), indicating that the reaction kinetics is mainly determined by diffusion-controlled characteristics.

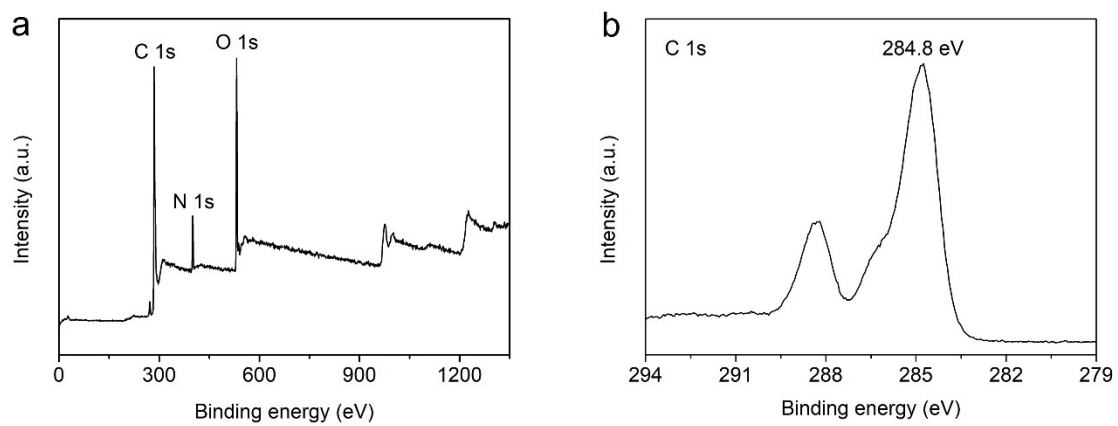


**Figure S21.** (a) XPS full spectra of pristine TPBQ. (b) High-resolution XPS C1s spectrum with the binding energy of 284.8 eV as the interior reference.

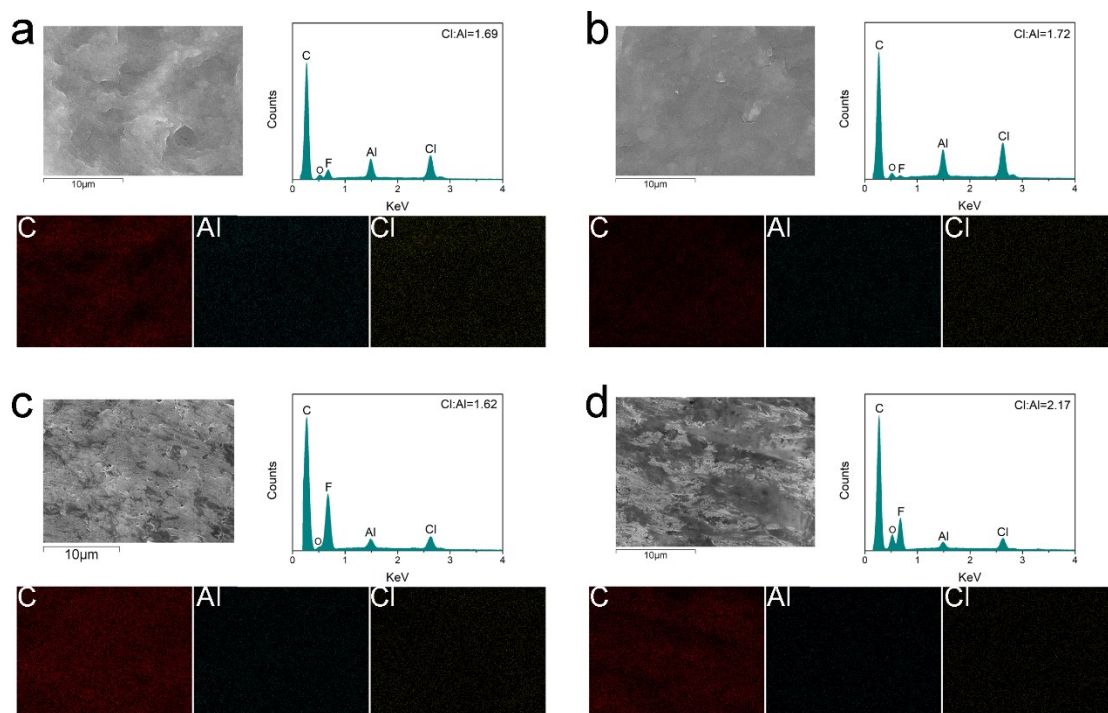


**Figure S22.** EDS spectra of various TPBQ electrodes discharged to 0.5V. The average ratio of Cl-to-Al approaches 1.8.

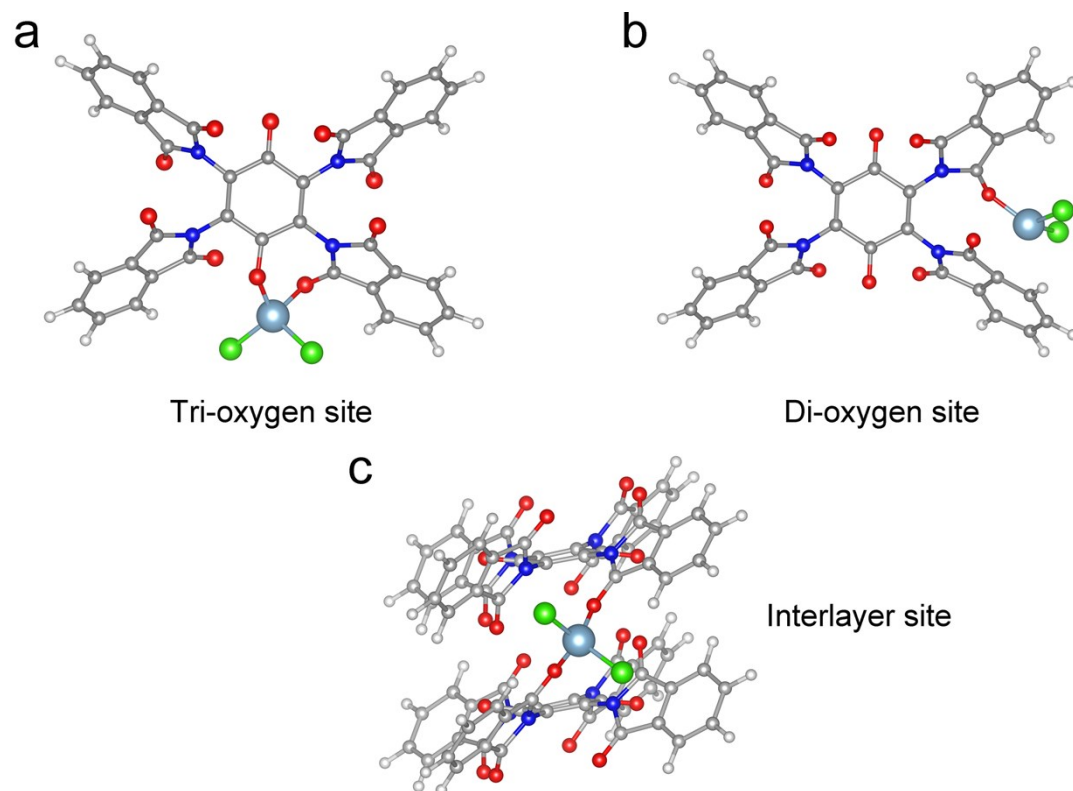


**Figure S23.** The simulated (a) Tri-oxygen, (b) Di-oxygen, and (c) Interlayer sites of TPBQ coordinated with  $\text{AlCl}_2^+$  by DFT calculations. In Tri-oxygen site, there are three carbonyl groups, two of which are coordinated with  $\text{AlCl}_2^+$ . While in Di-oxygen site, one out of two carbonyl groups is coordinated with  $\text{AlCl}_2^+$ . In interlayer site,  $\text{AlCl}_2^+$  is located at the interlayer of two TPBQ molecules and coordinated with two carbonyl groups.

In “Interlayer” site,  $\text{AlCl}_2^+$  is located between two TPBQ molecules and coordinated with two oxygen atoms forming a tetrahedron (Figure S23c). However, because of the limited space between “Interlayer” and “Di-oxygen” sites, there is less possibility for “Interlayer” sites coordinated with  $\text{AlCl}_2^+$  (Table S5-S7).

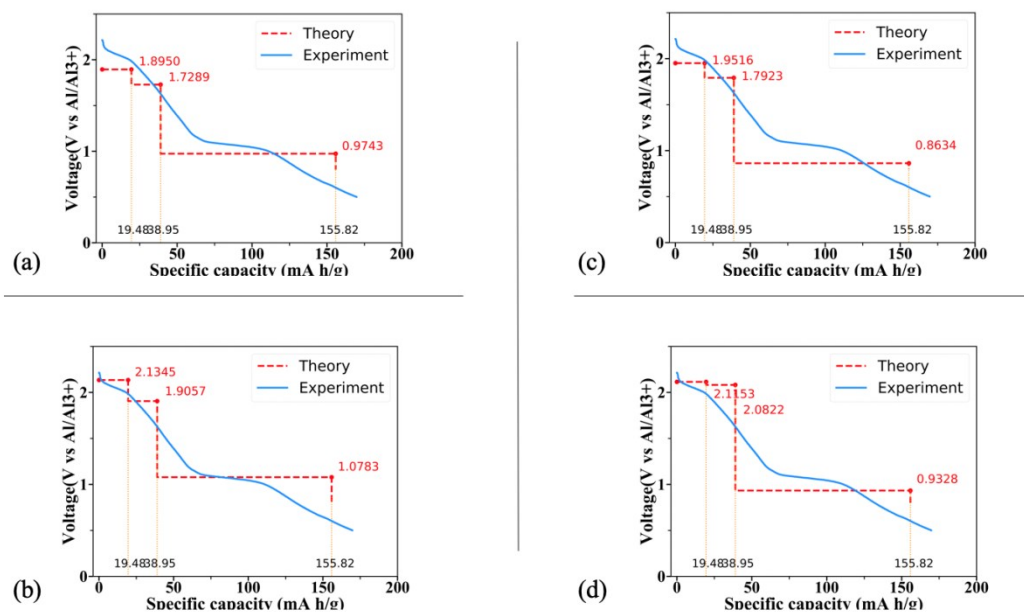
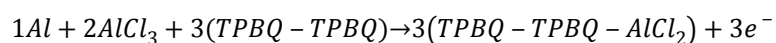


**Figure S24.** Comparison of the discharge voltage curves of four simulated TPBQ structures by DFT calculations: (a) "S-1n", (b) "S-1r", (c) "S-2n", and (d) "S-2r".

Figure S24 shows that in another less thermodynamically stable TPBQ confirmation, the voltages of each stage are slightly lower, but the overall capacity vs. voltage result is very similar.

**Table S5.** The discharge potential at different  $\text{AlCl}_2^+$  coordination sites of TPBQ with capacity of 19.48 mA h/g. Site T, D, and L represent is “Tri-oxygen” site; “Site D” is “Di-oxygen” site; “Site L” is “Interlayer” site (shown in Figure 6).

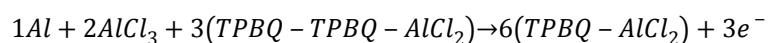


	Al	2AlCl <sub>3</sub>	3TPBQ-TPBQ	Total	3(TPBQ-TPBQ-AlCl <sub>2</sub> )	Binding energy	Potential (V)
S-1n			-3016.2	-3050.5	Site T: -1018.7*3	-5.69	1.90
					Site D: -1016.9*3	-0.08	0.03
					Site L: -1018.3*3	-4.36	1.45
S-1r	-3.73	-30.62	-3014.4	-3048.7	Site T: -1018.4*3	-6.40	2.13
					Site D: -1016.3*3	-0.03	0.01
					Site L: -1018.2*3	-5.85	1.95
S-2n			-3015.2	-3049.5	Site T: -1018.5*3	-5.85	1.95
					Site L: -1018.1*3	-4.70	1.57
S-2r			-3011.0	-3045.4	Site T: -1017.2*3 Site D:---	-6.35 ---	2.12 ---

Unit:

eV

**Table S6.** The discharge potential at different  $\text{AlCl}_2^+$  coordination sites of TPBQ with capacity of 38.48 mA h/g. Site T-T represents Tri-oxygen + Tri-oxygen site, while site T-D represents Tri-oxygen + Di-oxygen site.



	Al	2Al Cl <sub>3</sub>	3(TPBQ- TPBQ- AlCl <sub>2</sub> )	total	6(TPBQ-AlCl <sub>2</sub> )	Binding energy	Potenti al (V)
S-1n			-3056.2	-3090.5	Site T-T: -1031.87*3 Site T-D: -1031.91*3	-5.06 -5.19	1.69 1.73
S-1r	-3.73	30.	-3055.1	-3089.5	Site T: -1031.73*3	-5.72	1.91
S-2n		62	-3055.4	-3089.7	Site T-T: -1031.70*3 Site T-D: -1031.68*3	-5.38 -5.32	1.79 1.77
S-2r			-3051.7	-3086.0	Site T: -1030.77*3	-6.25	2.08

Unit:

eV

**Table S7.** The discharge potential at different  $\text{AlCl}_2^+$  coordination sites of TPBQ with capacity of 155.82 mA h/g.



	3Al	6AlCl <sub>3</sub>	3(TPBQ-AlCl <sub>2</sub> )	total	3(TPBQ-4AlCl <sub>2</sub> )	Binding energy (eV)	Potential (V)
S-1n			-1547.87	-1650.9	Site 1: -1106.44*1.5 Site 2: -1112.34*1.5	-8.77 -17.61	0.97 1.96
S-1r	-	-	-1547.6	-1650.6	Site 1: -1106.89*1.5	-9.70	1.08
S-2n	11.1	91.85	-1547.5	-1650.6	Site 1: -1105.57*1.5 Site 3: -1108.29*1.5	-7.77 -11.85	0.86 1.32
S-2r	8		-1546.1	-1649.2	Site 1: -1105.05*1.5	-8.39	0.93

Unit: eV

Site 1: (site T + site D)\*4

Site 2: (site T + site L)\*4

Site 3: [(site T)\*2 + (site D)\*1 + (site L)\*1]\*2

## References

1. Manivannan, R., Ciattini, S., Chelazzi, L. & Elango, K.P. Benzoquinone–imidazole hybrids as selective colorimetric sensors for cyanide in aqueous, solid and gas phases. *RSC Advances* **5**, 87341-87351 (2015).
2. Lin, J.-H. *et al.* Manufacturing techniques and property evaluations of conductive composite yarns coated with polypropylene and multi-walled carbon nanotubes. *Composites Part A: Applied Science and Manufacturing* **84**, 354-363 (2016).
3. Mao, M. *et al.* High-Energy-Density Rechargeable Mg Battery Enabled by a Displacement Reaction. *Nano Letters* **19**, 6665-6672 (2019).
4. Lindström, H. *et al.* Li<sup>+</sup> Ion Insertion in TiO<sub>2</sub> (Anatase). 2. Voltammetry on Nanoporous Films. *The Journal of Physical Chemistry B* **101**, 7717-7722 (1997).
5. Augustyn, V. *et al.* High-rate electrochemical energy storage through Li<sup>+</sup> intercalation pseudocapacitance. *Nature materials* **12**, 518 (2013).
6. Mao, M. *et al.* A Pyrazine-Based Polymer for Fast-Charge Batteries. *Angewandte Chemie* **131**, 17984-17990 (2019).